MICROCRYSTALLINE, NANOCRYSTALLINE, POROUS, AND COMPOSITE SEMICONDUCTORS

Manganese Clusterization in ZnS:Mn, Mg Synthesized by Self-Propagating High-Temperature Synthesis

Yu. Yu. Bacherikov[a],*, I. P. Vorona[a], O. B. Okhrimenko[a], V. P. Kladko[a], A. G. Zhuk[a], S. M. Okulov[a], Yu. O. Polishchuk[a], A. V. Gilchuk[b], Yu. M. Romanenko[b], and V. V. Kidalov[c]

[a] *Lashkaryov Institute of Semiconductor Physics, National Academy of Sciences of Ukraine, Kyiv, 03028 Ukraine*
[b] *National Technical University of Ukraine "Igor Sikorsky Kyiv Polytechnic Institute", Kyiv, 03506 Ukraine*
[c] *Berdyansk State Pedagogical University, Berdyansk, 71100 Ukraine*
*e-mail: yuyu@isp.kiev.ua

Abstract—The ZnS:Mn, Mg powder is fabricated by self-propagating high-temperature synthesis with the simultaneous introduction of Mn and Mg impurities. It is found that the simultaneous introduction of Mn and Mg impurities leads to the nonuniform distribution of manganese forming regions with a lower and higher Mn concentration. In the latter case, the manganese ions form paramagnetic clusters. At the same time, numerous centers of self-activated luminescence form in the synthesized ZnS:Mn, Mg due to mechanical stress and lattice strain. Additional annealing leads to a more uniform Mn distribution in the formed ZnS:Mn, Mg phosphor, which is accompanied by an increase in the intensity of the manganese photoluminescence band and quenching of the self-activated luminescence band.

1. INTRODUCTION

Zinc sulfide occupies an important place among semiconductor materials. This is due to a series of distinctive features such as a large band-gap width, ability to emit in the visible region under diverse external actions: mechanical, optical, X-ray, cathodoluminescence, electroexcitation, etc. In addition, its high sensitivity to these actions makes it possible to use ZnS as a sensor [1, 2]. Therefore, the development of new zinc sulfide-based composite structures can considerably extend its functional possibilities and application in microelectronics. In particular, composites consisting of ZnS and nanoparticles of metals possessing magnetic properties are related to such structures. Manganese is one of the most suitable magnetic impurities in ZnS due to its high solubility and diffusion ability. Theoretical investigation into the behavior of atomic clusters of transition metals showed [3] that manganese clusters should have a considerable magnetic moment and manifest ferromagnetic properties. This fact was later confirmed experimentally for small-size manganese clusters Mn_n ($n = 11-99$) [4].

It should be noted that the fabrication of composite nanostructures including metallic clusters with ferromagnetic properties is a rather complex problem. As a rule, metallic clusters can be prepared by a limited number of methods, notably, laser deposition, metal evaporation and condensation in a plasma flow with the injection of the substance binding the particles, the formation of cluster beams, etc. [5–7]. All these methods are rather complex technically and high cost. Therefore, in order to form composite nanostructures with a complex internal structure, it is necessary to approve new methods material synthesis such as self-propagating high-temperature synthesis (SHS), which appeared not so long ago [8, 9]. The advantage of this method is its simplicity and low cost, which makes it possible to make the prepared materials considerably less expensive. In addition, the variation in synthesis modes makes it possible to fabricate materials with different stoichiometry, different structure (wurtzite, sphalerite), particle sizes, etc. Magnesium or its salts can be used as the reagent, which promotes the appearance of metallic clusters in zinc sulfide, to activate the desulfuration processes.

In addition, it was found that additional doping with magnesium improves the electroluminescence characteristics of thin-film devices based on ZnS:Cu and ZnS:Mn and also leads to an increase in the photoluminescence (PL) intensity of zinc sulfide [10, 11].

The preparation of a highly efficient phosphor and photoconductor with clearly pronounced ferromagnetic properties will make it possible to substantially extend the functional possibilities of ZnS, which
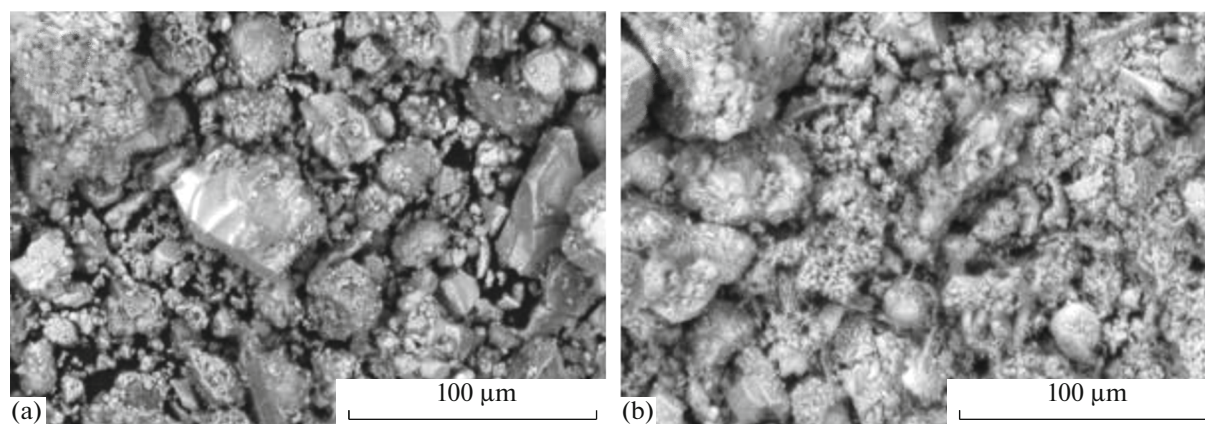
Fig. 1. SEM images in secondary electrons of the (a) initial powder ZnS:Mn, Mg-SHS and (b) that annealed at 800°C.

determines the topicality of this work. The goal of this work is to fabricate composite materials consisting of Mn clusters in a ZnS matrix in one process cycle by self-propagating high-temperature synthesis (SHS) and modify these clusters during subsequent heat treatment of the material, as well as to study its luminescent and paramagnetic properties before and after the thermal effect.

2. EXPERIMENTAL

Finely dispersed ZnS:Mn was synthesized by SHS [8, 9]. Doping by manganese and magnesium was performed directly during synthesis. Zinc and sulfur were taken in a stoichiometric ratio, while the Mn and Mg impurity concentrations in the charge were ~1.2 and 5 wt %, respectively.

SHS-fabricated ZnS:Mn, Mg (further denoted as ZnS:Mn, Mg-SHS) was annealed in a laboratory furnace at 800°C for 120 min (cooling with a furnace). To limit exposure to air, a gas gate made of granulated activated carbon was used.

The photoluminescence (PL) spectra and luminescence excitation (LES) spectra were recorded at room temperature using an SDL-2 installation. When recording the LES and PL, the luminescence was excited by the radiation of a DKSSh-150 xenon lamp passed through an MDR-12 monochromator.

The morphology and local elemental composition of the powders was analyzed by scanning electron microscopy using an REM-106 microscope (SELMI) equipped with an energy-dispersive X-ray spectrometer. The measurements were performed at an accelerating voltage of 20 kV.

X-ray diffraction was investigated using a Philips X'Pert-MRD diffractometer (CuK_α, wavelength λ = 0.15418 nm) in the Bragg−Brentano geometry. The size of the coherent scattering regions D_{hkl} (hkl are the Miller indices of the reflecting planes) was determined according to the Scherrer formula $D_{hkl} = 0.9\lambda/\beta_{hkl}\cos\theta$,

where λ is the radiation wavelength, β_{hkl} is the angular reflection width at half-maximum, and θ is the angular peak position. To determine β_{hkl} more exactly, the peaks were approximated by a pseudo-Voigt function. The composition was evaluated quantitatively by the method of corundum numbers.

The EPR investigations were performed at room temperature using a Varian E-12 X-range spectrometer.

3. RESULTS AND DISCUSSION

The scanning electron microscopy data of the synthesized and annealed ZnS:Mn, Mg-SHS powders (Fig. 1) showed no clear variation in the powder particle sizes before and after annealing. However, the finest phase after annealing is more conglomerated, which can be caused by partial powder sintering during annealing.

The X-ray diffraction patterns of the initial and annealed powders are shown in Fig. 2. Their analysis shows that the initial powder consists mainly of the hexagonal (2H) zinc-sulfide phase and metallic zinc. The amount of ZnS and Zn [12] in the mixture evaluated by the method of corundum numbers is approximately 65 and 35%, respectively. In addition, a small amount of sulfur is also present in the material, which is evidenced by a series of weak peaks in the range $2\theta \approx$ 23−28.

Annealing leads to a change in the phase composition of the powder. It is seen in Fig. 2 that the cubic ZnS phase becomes dominant after annealing, but the hexagonal ZnS phase is also present. Their amount is 78 and 12%, respectively [12].

In addition, the powder contains ~10% of zinc oxide ZnO [12]. No metallic zinc as well as sulfur traces are observed after annealing.

The variation in the phase composition of the powder-like ZnS during annealing is accompanied by a change in the coherent-scattering region (D). The val-

ues of these quantities are assessed according to the Scherrer formula [13] and are presented in Table 1.

The elemental compositions of the initial and annealed powders determined by energy dispersive X-ray spectral analysis are presented in Table 2. The calibration procedure using standards was performed before the measurements. The measurement error was ~30% for Mg, ~2% for S, ~10% for Cl, ~25% for Mn, and ~2% for Zn. It is seen from the results that the initial powder contains almost equal amounts of zinc and sulfur in atomic ratio. However, a considerable part of the elements was unreacted according to the results of analysis of the phase composition (Table 1). Sulfur actively evaporated during annealing, which led to a relative increase in the atomic content of Mn and Mg. In addition, metallic zinc partially reacted and partially oxidized with the formation of ZnO (Fig. 2).

An increase in the atomic content of sulfur with a simultaneous increase in the Mn and Mg content is explained by different values of the specific heat of evaporation ΔH of the corresponding elements. It was 10.5 kJ/mol for sulfur and 114.8, 221, and 131.8 kJ/mol for Zn, Mn, and Mg, respectively [14]. The evaporation intensity is proportional to $\exp(-\Delta H/kT)$. Thus, a more than tenfold difference in the specific heat of evaporation for sulfur and magnesium (manganese) during prolonged annealing leads to the active evaporation of sulfur, due to which, the relative content of Mg and Mn increases.

Figure 3a shows the PL spectra of powder-like ZnS:Mn, Mg-SHS before (curve 1) and after annealing at 800°C (curve 2). It is seen in Fig. 3 (curve 1) that the PL spectrum of ZnS:Mn, Mg-SHS before annealing consists of two bands with $\lambda_{max} \sim 460$ and 590 nm, and the band with $\lambda_{max} \sim 460$ nm is dominant. The latter is the superposition of several bands caused by SA luminescence centers [15]. As a rule, the introduction of Mn into ZnS leads to a decrease in the intensity of the SA luminescence bands and the appearance of a broad orange band peaked at $\lambda_{max} \sim 590$ nm [16, 17].

The band with $\lambda_{max} \sim 460$ nm (curve 1, Fig. 3a) consists of at least three individual bands with $\lambda_{max} \sim$ 435, 465, and 515 nm. The band with $\lambda_{max} \sim 435$ nm can be associated with the presence of oxygen [18, 19] or chlorine [20] in ZnS. It was shown [20] that the luminescence band with $\lambda_{max} \sim 470$ nm, which is characteristic of ZnS(Cl), is nonelementary and consists of bands with $\lambda_{max} = 496, 466, 426$, and 405 nm. According to [15, 20], the bands with $\lambda_{max} = 496, 466, 426,$ and 405 nm are associated with the centers by the $V_{zn}Cl_S$ associant—Zn_i, Cl_S, and V_S, respectively. The band with $\lambda_{max} \sim 515$ nm is usually associated with a sulfur excess in ZnS crystals [21].

The PL band with $\lambda_{max} \sim 590$ nm is characteristic of ZnS doped with Mn. It also consists of several overlapping separate bands with $\lambda_{max} \sim 557, 578, 600,$ and 630 nm. According to [22, 23], the band with $\lambda_{max} \sim$
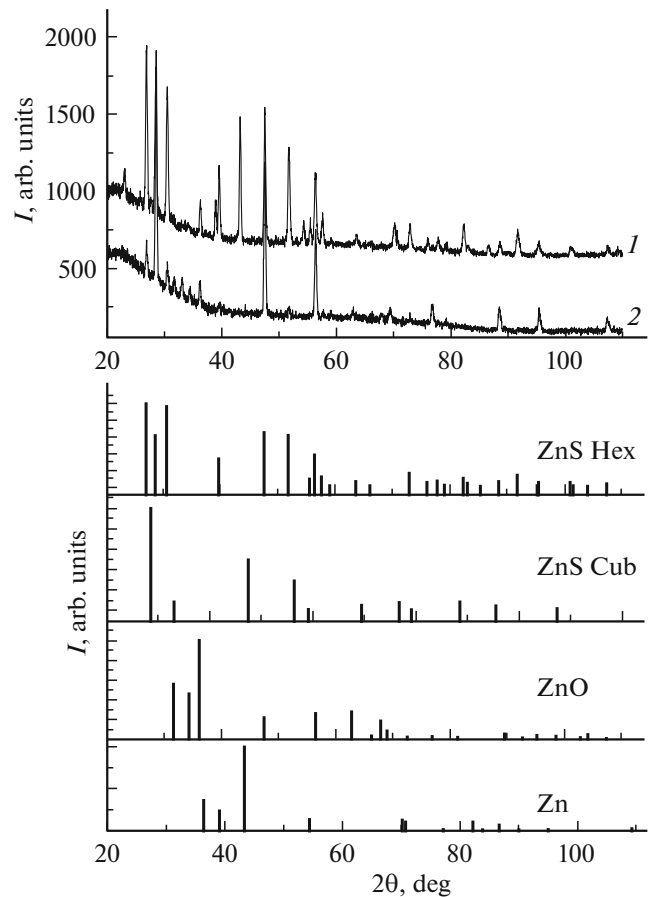

Fig. 2. X-ray diffraction spectrum of powder ZnS:Mn, Mg-SHS (1) before and (2) after annealing. The standard X-ray diffraction patterns of the main phases in the materials are shown at the bottom.

600 nm is caused by a radiative transition in Mn^{2+} ions, which are arranged in octahedral interstices, while the band with $\lambda_{max} \sim 578$ nm is associated with a radiative transition in Mn^{2+} ions arranged near dislocations or point defects. The PL band with $\lambda_{max} \sim$ 630 nm is related to Mn in the α-MnS phase [24], which was not dissolved in the ZnS lattice, or with inclusions of the MnS phase with a large amount of

Table 1. Phase composition and coherent-scattering region of ZnS:Mn, Mg-SHS before and after annealing

Phases	Initial		Annealed	
	content in the volume, %	D, nm	content in the volume, %	D, nm
$2H$-ZnS	65	24.1	12	30.4
$3C$-ZnS	—	—	78	24.9
Zn	35	34.3	—	—
S	<1		—	—
ZnO	—	—	10	29.6

Table 2. Elemental composition of the initial and annealed ZnS:Mn, Mg-SHS

	Zn, at %	S, at %	Mn, at %	Mg, at %	Cl, at %
Initial	51.34	44.02	0.31	1.46	1.96
Annealed	61.64	33.66	0.59	3.21	0.18

Mn in zinc sulfide. Most authors (for example, [25, 26]) associate the band with $\lambda_{max} \sim 557$ nm with the centers formed by manganese ions arranged in the Zn sublattice at sites near local lattice distortions and violations.

It is seen in Fig. 3a that the presence of Mg in ZnS does not affect the spectral characteristics of the PL. This fact agrees with the data of [27, 28], where it was shown that the introduction of Mg into ZnS leads to a considerable increase in the PL brightness without varying its spectral characteristics. The increase in the brightness of the radiation of ZnS:Mg is conditioned by the partial filling of tetrahedral interstices and/or the substitution of zinc by magnesium ions [18]. This leads to the appearance of mechanical stresses in the ZnS lattice and increases the amount of intrinsic defects including those responsible for SA luminescence.

It is noteworthy that the shape of the PL spectra of ZnS:Mn, Mg-SHS immediately after synthesis better fits zinc sulfide lightly doped with manganese with the Mn content lower than several tenths of a percent [16, 17]. As a rule, if the manganese content in ZnS is more than 1%, then the band peaked in the region of 590 nm dominates, while the bands of the SA PL are pronounced weakly or absent [17].

When simultaneously introducing Mn and Mg during SHS, the competition of manganese both with zinc and with magnesium during its incorporation into the zinc-sulfide lattice should be taken into account (in the rapidly varying synthesis and crystallization conditions of ZnS). This case is close to that of the nonstoichiometric ratio of the components in the charge during SHS when the zinc excess in the charge is <10% [16]. This is caused by desulfuration processes associated with the presence of the magnesium impurity. In the case of introducing magnesium, due to its high reaction ability, Mg easily forms compounds with oxygen and sulfur displacing less active Zn and Mn. In addition, magnesium sulfide is formed at 500−600°C, while the formation temperature for MnS is ~1000°C. The lower formation temperature of MgS and the ability of Mg to replace less reactive metals in compounds with sulfur can lead to the complicated introduction of Mn into the ZnS lattice and promote its precipitation in the form of a metallic phase, i.e., to the formation of manganese clusters. This is indirectly confirmed by the low intensity of the PL band with $\lambda_{max} \sim 590$ nm as well as by the EPR data presented below.

It is well known that additional treatment, such as thermal annealing, promotes a more uniform distribution of doping impurities in the host lattice. It is seen from Fig. 3 that the annealing of ZnS:Mn, Mg-SHS leads to considerable redistribution of the PL bands. The band with a maximum up to 590 nm becomes dominant in the PL spectra after annealing. This band corresponds to the radiative transition in Mn^{2+} ions. At the same time, the intensity of the SA PL decreased by a factor of 15 relative to the band associated with Mn.

The LES of the ZnS:Mn, Mg-SHS synthesized and annealed at 800°C, which were normalized by the maximum of the band-to-band excitation band are presented in Fig. 3b (curves *1*, *2*). The LES of the
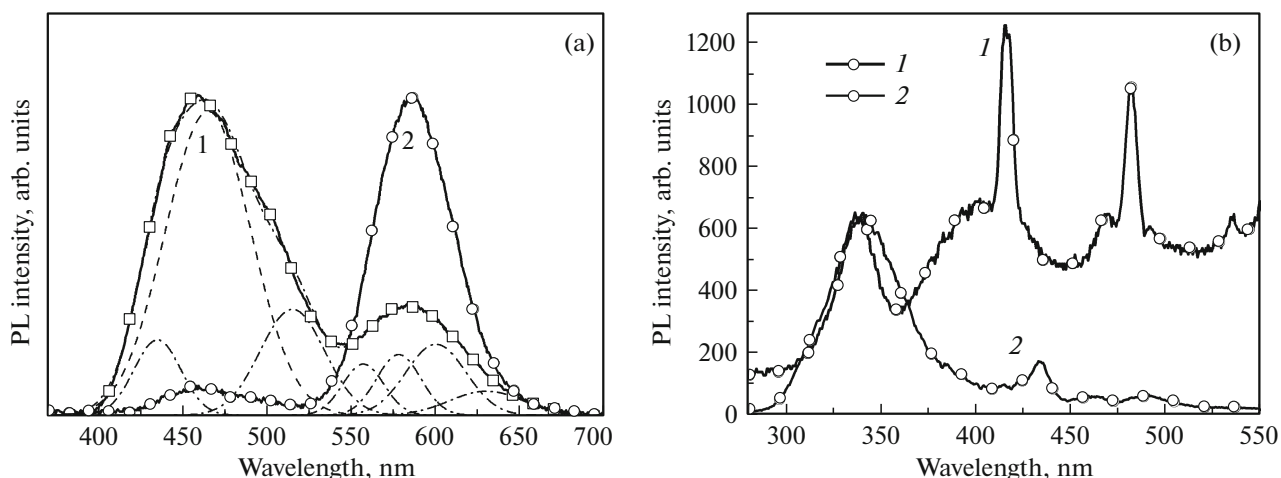
Fig. 3. PL spectra with (a) $\lambda_{exc} = 337$ nm and (b) LES PL bands with $\lambda_{max} = 580$ nm of (*1*) initial and (*2*) annealed powder ZnS:Mn, Mg-SHS. The PL spectra are normalized by their intensity maximum. The LES spectra are normalized by the maximum of the fundamental excitation band.
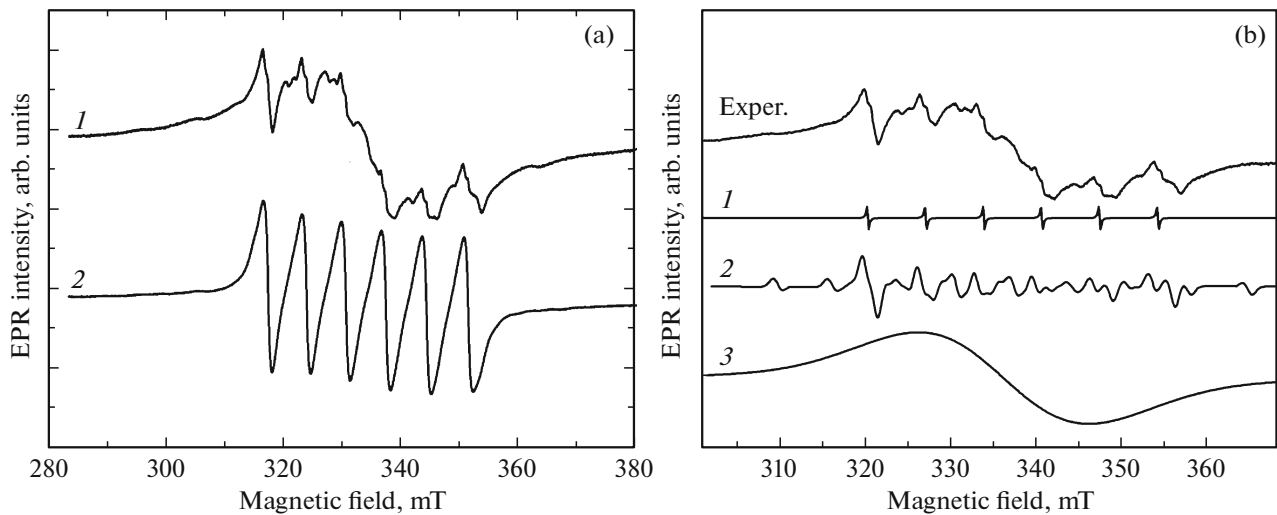
Fig. 4. (a) EPR spectra of ZnS:Mn, Mg-SHS (*1*) before and (*2*) after annealing at 800°C. (b) Decomposition of the spectrum of the initial material into components: (*1*) Mn^{2+}_{Zn} in the cubic ZnS lattice, (*2*) Mn^{2+}_{Zn} in the hexagonal ZnS lattice, and (*3*) Mn^{2+} ions coupled by the strong exchange interaction (manganese clusters).

ZnS:Mn, Mg-SHS contains a band with $\lambda_{max} \sim$ 340 nm associated with fundamental absorption in ZnS, as well as bands with $\lambda_{max} \sim$ 419, 435, 468, and 493 nm corresponding to the known [29−31] manganese LES bands. The latter are caused by the intracenter transitions of Mn^{2+} ions from the ground state A_1 to the excited states $^4T_1$, $^4T_2$, $^4E_1$, and $^4A_1$ [30, 31]. It is seen from Fig. 3b (curve *1*) that the LES bands associated with Mn^{2+} are pronounced weakly and are much weaker than the fundamental absorption band, which points to a low concentration of Mn entering ZnS sites. The spectrum substantially changes after annealing, notably, the bands caused by Mn^{2+} dominate in the LES (curve *2*). This fact evidences an increase in the atomic content of Mn in the annealed ZnS:Mn, Mg-SHS and agrees well with the EDS data (Table 2). The different position of the Mn-conditioned bands in curves *1* and *2* is associated with the different localization of Mn in the zinc-sulfide lattice before and after annealing. The spread of the ZnS-band edge in curve *1* (Fig. 3b) when compared with curve *2* is due to the higher Cl concentration because the presence of Cl in ZnS leads to the appearance of a set of shallow levels located near the conduction-band bottom [32].

Figure 4 shows the EPR spectra of the ZnS:Mn, Mg-SHS before and after annealing at 800°C. The EPR spectrum of the ZnS:Mn, Mg powder before annealing is a typical EPR spectrum of Mn^{2+} ions in heavily doped ZnS:Mn powders, which has a mixed phase composition (see, for example, [16]). It contains three components caused by Mn^{2+} ions with different localization in the material. The first component (signal *1*), which has the minimal intensity, consists of six regularly shaped lines with equal intensities. This is due to Mn^{2+} ions substituting Zn (Mn^{2+}_{Zn} ions) in the ZnS cubic lattice. It is noteworthy that X-ray structural analysis did not reveal the cubic zinc-sulfide phase in this material. This can be explained by the higher sensitivity of the Mn^{2+} EPR signal to the presence of the cubic phase in ZnS [33]. The second component (signal *2*) is a complex EPR signal, which consists of six more intense irregularly shaped lines in the spectrum center and a series of less intense lines between them and on the sides. This signal is characteristic of the Mn^{2+}_{Zn} substitutional ions in the ZnS hexagonal lattice. The last, most intense component (signal *3*), is an approximately symmetric wide single line. It is also caused by Mn^{2+} ions, but their arrangement is disputable. It is usually prescribed to ions arranged in a highly imperfect region or a region with a high local concentration of manganese ions connected by dipole−dipole or exchange interaction. A similar EPR line was also repeatedly observed for other manganese-doped II−VI materials. In particular, it was shown in magnetization and EPR measurements in CdS:Mn performed at various temperatures [34−36] that the variation in the intensity of this line with temperature does not follow the Curie−Weiss law. Based on these investigations, it was attributed to manganese clusters connected by strong exchange interaction and demonstrating superparamagnetic properties. It is noteworthy that similar properties (ability to form superparamagnetic clusters) are inherent to other impurities, in particular, copper in zinc sulfide [37, 38].

The presence of several EPR signals points to non-uniform manganese distribution in the synthesized material. A part of manganese ions substitute zinc ions in the cation sublattice of zinc sulfide, while most

Mn^{2+} ions are associated with a strong exchange interaction and form superparamagnetic clusters. The presence of such clusters can explain the low intensity of luminescence associated with Mn because a larger part of manganese, when forming the cluster, is excluded from radiative-recombination processes.

The EPR signal of the annealed powder comprises one signal consisting of six lines with identical intensity. It seems likely that this is caused by Mn_{Zn}^{2+} ions, but it is impossible to determine exactly, for which type of substitutions (cubic or hexagonal), because of broadening of the lines caused by the dipole−dipole interaction of Mn^{2+} ions. The appearance of such broadening points to an increase in the number of Mn_{Zn} ions.

Thus, annealing leads to a uniform manganese distribution in the material due to the diffusion of Mn^{2+} ions from regions with their high local concentration, which is evidenced by the disappearance of the broad band in the EPR spectrum of the annealed powder and considerable increase in the intensity of the LES bands caused by Mn^{2+} with respect to the intensity of the LES band caused by the band-to-band transition. In addition, the high-temperature annealing of ZnS:Mn, Mg-SHS promotes the incorporation of manganese into cationic sites of the ZnS lattice (an increase in the intensity and line width of the corresponding EPR signal).

It is noteworthy that the annealing of powder-like ZnS:Mn, Mg-SHS was performed at a rather high temperature of 800°C for 120 min. This mode promotes the uniform distribution of Mn atoms in the ZnS sublattice. At the same time, the selection of other heat-treatment modes will possibly lead to the modification of manganese clusters and the formation of clusters with other paramagnetic properties, but this hypothesis requires additional investigations.

CONCLUSIONS

Thus, the use of $MgCl_2$ as the doping impurity during the SHS synthesis of ZnS:Mn makes it possible to form metallic Mn clusters with magnetic properties. The formation of manganese clusters is confirmed by the appearance of a superparamagnetic EPR signal and explains the weak intensity of the bands in the PL and SHS spectra associated with Mn. Prolonged thermal annealing leads to the complete dissolution of metallic clusters, the incorporation of Mn into the ZnS lattice, and an increase in the concentration of Mn_{Zn}^{2+} ions. This improves the powder as a luminescent material (the intensity of the PL band associated with Mn increases) and is accompanied by a change in its phase composition—the 2H-ZnS phase dominates in the initial material, while the annealed powder contains 12% 2H-ZnS and 78% 3°C-ZnS.

CONFLICT OF INTEREST

The authors declare that they have no conflict of interest.

REFERENCES

1. I. K. Sou, Z. H. Ma, Z. Q. Zhang, and G. K. L. Wong, J. Cryst. Growth **214−215**, 1125 (2000).

2. M. P. Sarma, J. M. Kalita, and G. Wary, Mater. Sci. Semicond. Proc. **61**, 131 (2017).

3. S. K. Nayak and P. Jena, Chem. Phys. Lett. **289**, 473 (1998).

4. M. B. Knickelbein, Phys. Rev. Lett. **86**, 5255 (2001).

5. R. L. Johnston, *Atomic and Molecular Clusters* (Taylor and Francis, London, 2002).

6. J. S. Becker and H. J. Dietze, J. Anal. Chem. **359**, 338 (1997).

7. H. Pauly, *Atom, Molecule, and Cluster Beams I: Basic Theory, Production and Detection of Thermal Energy Beams* (Springer, Germany, 2000).

8. V. S. Trofimov and E. V. Petrov, Int. J. Self-Propag. High-Temp. Synth. **23**, 187 (2014).

9. S. T. Aruna and A. S. Mukasyan, Curr. Opin. Solid-State Mater. Sci. **12**, 44 (2008).

10. S. H. Ryu, W. K. Kim, and S. E. Lee, Trans. Electric. Electron. Mater. **14**, 24 (2013).

11. J. Yuan, D. Haneman, and B. Gong, Mater. Res. Innov. **2**, 223 (1999).

12. ICDD The International Centre for Diffraction Data. www.icdd.com.

13. A. L. Patterson, Phys. Rev. **56**, 978 (1939).

14. G. W. C. Kaye and T. H. Laby, *Tables of Physical and Chemical Constants* (Longman, London, New York, 1986).

15. *Physics and Chemistry of II−VI Compounds*, Ed. by M. Aven and J. S. Prener (North-Holland, Amsterdam, New York, 1967).

16. Yu. Yu. Bacherikov, N. P. Baran, I. P. Vorona, A. V. Gilchuk, A. G. Zhuk, Yu. O. Polishchuk, S. R. Lavorik, V. P. Kladko, S. V. Kozitskii, E. F. Venger, and N. E. Korsunska, J. Mater. Sci.: Mater. Electron. **28**, 8569 (2017).

17. Yu. Yu. Bacherikov, I. Vorona, A. Zhuk, A. V. Gilchuk, N. Korsunska, and I. Markevich, Semicond. Sci. Technol. **32**, 1 (2017).

18. N. K. Morozova, I. A. Karetnikov, V. V. Blinov, and E. M. Gavrishchuk, Semiconductors **35**, 24 (2001).

19. J. Díaz-Reyes, R. S. Castillo-Ojeda, R. Sanchez-Espíndola, M. Galvan-Arellano, and O. Zaca-Moran, Curr. Appl. Phys. **15**, 103 (2015).

20. V. F. Tunitskaya, T. F. Filina, E. I. Panasyuk, and Z. P. Ilyukhina, Zh. Prikl. Spektrosk. **14**, 239 (1971).

21. N. K. Morozova, I. A. Karetnikov, K. V. Golub, N. D. Danilevich, V. M. Lisitsyn, and V. I. Oleshko, Semiconductors **39**, 485 (2005).

22. N. D. Borisenko, M. F. Bulanyi, F. F. Kodzhespirov, and B. A. Polezhaev, Zh. Prikl. Spektrosk. **55**, 452 (1991).

23. M. F. Bulanyi, B. A. Polezhaev, and T. A. Prokof'ev, Semiconductors **32**, 603 (1998).

24. N. Karar, F. Singh, and B. R. Mehta, J. Appl. Phys. **95**, 656 (2004).

25. M. F. Bulanyi, B. A. Polezhaev, T. A. Prokof'ev, and I. M. Chernenko, J. Appl. Spectrosc. **67**, 282 (2000).

26. W. Busse, H. Gumlish, and R. O. Tornqvist, Phys. Status Solidi A **76**, 553 (1983).

27. L. M. Dong, M. J. Li, X. D. Liu, K. J. Wu, and Y. K. Guo, J. Ovonic Res. 12, 155 (2016).

28. H. Joy Prabu, and I. Johnson, Int. J. Eng. Res. Appl. **5**, 99 (2015).

29. D. A. Reddy, D. H. Kim, S. J. Rhee, B. W. Lee, and C. Liu, Nanoscale Res. Lett. **9**, 20 (2014).

30. T. A. Prokof'ev, B. A. Polezhaev, and A. V. Kovalenko, J. Appl. Spectrosc. **72**, 865 (2005).

31. V. F. Agekyan, Phys. Solid State **44**, 2013 (2002).

32. Yu. Yu. Bacherikov, Phys. Solid State **52**, 1653 (2010).

33. V. Nosenko, I. Vorona, V. Grachev, S. Ishchenko, N. Baran, Yu. Bacherikov, A. Zhuk, Yu. Polishchuk, V. Kladko, and A. Selishchev, Nanoscale Res. Lett. **11**, 517 (2016).

34. C. Barglik-Chory, C. Remenyi, C. Dem, M. Schmitt, W. Kiefer, C. Gould, C. Rüster, G. Schmidt, D. M. Hofmann, D. Pfisterer, and G. Muler, Phys. Chem. Chem. Phys. **5**, 1639 (2003).

35. N. Feltin, L. Levy, D. Ingert, and M. P. Pileni, J. Phys. Chem. B **103**, 4 (1999).

36. G. Counio, S. Esnouf, T. Gacoin, and J.-P. Boilot, J. Phys. Chem. **100**, 20021 (1996).

37. J. D. Bryan and D. R. Gamelin, Progr. Inorg. Chem. **54**, 47 (2005).

38. Yu. Yu. Bacherikov, I. P. Vorona, A. A. Konchits, S. V. Optasyuk, S. V. Kozitskiy, and K. D. Kardashov, Funct. Mater. **17**, 158 (2010).

Translated by N. Korovin